Structural basis for the interaction of Asf1 with histone H3 and its functional implications

Florence Mousson*†, Aurélie Lautrette*, Jean-Yves Thuret‡, Morgane Agez*, Régis Courbeyrette‡, Béatrice Amigues*, Emmanuelle Becker*, Jean-Michel Neumann*, Raphaël Guerois*, Carl Mann‡§¶, and Françoise Ochsenbein*¶

*Service de Biophysique des Fonctions Membranaires and ‡Service de Biochimie et de Génétique Moléculaire, Département de Biologie Joliot-Curie, Commissariat à l'Energie Atomique (CEA/Saclay), F-91191 Gif-sur-Yvette, France

Edited by Gary Felsenfeld, National Institutes of Health, Bethesda, MD, and approved March 17, 2005 (received for review January 7, 2005)

Asf1 is a conserved histone chaperone implicated in nucleosome assembly, transcriptional silencing, and the cellular response to DNA damage. We solved the NMR solution structure of the N-terminal functional domain of the human Asf1a isoform, and we identified by NMR chemical shift mapping a surface of Asf1a that binds the C-terminal helix of histone H3. This binding surface forms a highly conserved hydrophobic groove surrounded by charged residues. Mutations within this binding site decreased the affinity of Asf1a for the histone H3/H4 complex *in vitro*, and the same mutations in the homologous yeast protein led to transcriptional silencing defects, DNA damage sensitivity, and thermosensitive growth. We have thus obtained direct experimental evidence of the mode of binding between a histone and one of its chaperones and genetic data suggesting that this interaction is important in both the DNA damage response and transcriptional silencing.

Asf1 histone chaperone | chromatin | DNA damage | NMR chemical shift mapping | nucleosome assembly

DNA in eukaryotic cells is packaged as nucleosome core particles containing ≈145 bp of DNA wrapped around an octamer comprised of two copies each of histones H2A, H2B, H3, and H4 (1). Assembly of histones into nucleosomes is a tightly orchestrated process (2, 3). Asf1 is a highly conserved histone chaperone that has been linked to both nucleosome assembly and disassembly (4–7). Asf1 interacts with two functional classes of protein: chromatin components, including histone H3 (8), the Hir proteins (9, 10), and the second subunit of CAF-I (5, 11, 12), and checkpoint kinases, including the Rad53 checkpoint kinase in budding yeast (13, 14) and the Tousled-like kinases in metazoans (15). The function of most of these interactions has not been defined. However, a Hir binding region of Asf1 was implicated in telomeric silencing but not required for resistance to genotoxic stress (16). Further work is necessary to determine the functional role of the remaining interactions and, in particular, for defining which Asf1 partners are required for the DNA damage response and for optimal cell growth. In this work, we present the solution structure of the functional N-terminal domain of human Asf1a, and we identify its histone H3 binding site. We show that Asf1 mutants severely defective in histone H3/H4 binding are incompetent in silencing and in providing resistance to DNA damage.

Methods

Protein Production. pETM30 allowed the production of recombinant $(His)_6$-GST-Tev site-fusion proteins in *Escherichia coli* strain BL21 gold (λDE3). Unlabeled and uniformly labeled proteins were obtained as described in ref. 17. After Tev cleavage, the ^{15}N-labeled-H3 (122–135) peptide was further purified by reverse-phase chromatography. The NMR buffer was described in ref. 17. An unlabeled peptide spanning the 122–133 sequence of histone H3 was obtained by chemical synthesis (Epytop, Nîmes, France). The protein concentrations were precisely measured by amino acid analysis.

NMR Structure Determination and Binding Experiments. NMR experiments were carried out on a Bruker DRX-600 spectrometer equipped with a triple-resonance broadband inverse probe or a cryoprobe. ^{1}H, ^{15}N, and ^{13}C resonance assignments were obtained as described in ref. 17. Peak intensities of the ^{15}N- and ^{13}C-edited 3D NOESY-heteronuclear single quantum correlation (HSQC) spectra (with a mixing time of 120 ms) were converted to distance restraints by using ARIA (ambiguous restraints for iterative assignment) (18, 19). One hundred thirteen (ϕ,ψ) restraints were derived by using TALOS (20) and 57 ϕ restraints by using $^3J_{HNH\alpha}$ couplings constants derived from the 3D HNHA spectrum (21); on the basis of the empirical Karplus relation, they were set to $-60 \pm 40°$ for $J_{HN\text{-}Ha} < 6$ Hz and to $-120 \pm 60°$ for $J_{HN\text{-}Ha} > 8$ Hz. An overview of the constraints is given in Table 1, which is published as supporting information on the PNAS web site. ARIA was used to calculate 20 structures, starting from random conformations with the standard procedure. Cumulative chemical shift variation upon binding was calculated as $\Delta\delta = [(\delta_{HN}{}^b - \delta_{HN}{}^f)^2 + (2.75(\delta_{H\alpha}{}^b - \delta_{H\alpha}{}^f))^2 + (0.17(\delta_N{}^b - \delta_N{}^f))^2]^{1/2}$, where b and f refer to the bound and free form, respectively. The scaling factors normalize the magnitude of the ^1H_N, $^1H\alpha$, and ^{15}N chemical shift changes (in ppm) (22). These factors were established from estimates of atom-specific chemical shift ranges in proteins: 5.5 ppm for ^1H_N, 2 ppm for $^1H\alpha$, and 32 ppm for ^{15}N. Assignments of the HSQC spectra of complexed Asf1 (1–156) and H3 (122–135) were obtained with 3D ^{15}N edited NOESY-HSQC and total correlation spectroscopy-HSQC spectra.

Phenotypic Testing of *asf1* Mutants. Wild-type and *asf1* mutants containing a 13myc C-terminal tag were expressed from the endogenous *ASF1* promoter on the centromeric *TRP1* vector pRS314. These plasmids were introduced into the following four yeast strains to test their ability to complement the DNA damage sensitivity, the thermosensitive growth defect, and the transcriptional silencing defect of *asf1*Δ or *asf1*Δ *cac2*Δ mutants. UCC6562 (a generous gift of Dan Gottschling, Fred Hutchinson Cancer Research Center, Seattle) = *Matα ade2*Δ*::hisG lys2Δ0 met15Δ0 trp1-Δ63 his3Δ200 ura3-52 leu2Δ0 DIA5-1 ppr1::LYS2 adh4::TEL(VIIL)-URA3 asf1::HIS3*; CMY1317 = as for

BIOCHEMISTRY

This paper was submitted directly (Track II) to the PNAS office.

Abbreviation: TAP, tandem affinity purification.

Data deposition: The atomic coordinates and structure factors for human Asf1a have been deposited in the Protein Data Bank, www.pdb.org (PDB ID code 1TEY). The NMR chemical shifts for human Asf1a have been deposited in the BioMagResBank, www.bmrb.wisc.edu (accession no. 6298).

†Present address: Department of Physiological Chemistry, Division of Biomedical Genetics, University Medical Center Utrecht, Universiteitsweg 100, 3584CG Utrecht, The Netherlands.

§Present address: Department of Biochemistry and Molecular Biology, F. Edward Hébert School of Medicine, Uniformed Services University of the Health Sciences, 4301 Jones Bridge Road, Bethesda, MD 20814-4799.

¶To whom correspondence may be addressed. E-mail: cmann@usuhs.mil or ochsenbe@dsvidf.cea.fr.

UCC6562, but *asf1*::*HIS3 cac2*::*kanMX*; CMY1312 = *Matα ade2-101 lys2-801 trp1-Δ63 his3Δ200 ura3-52 leu2Δ1 hmlα*::*URA3 asf1*::*HIS3 cac2*::*kanMX;* CMY1314 = *Matα ade2-101 lys2-801 trp1-Δ63 his3Δ200 ura3-52 leu2Δ1 hmrα*::*URA3 asf1*::*HIS3 cac2*::*kanMX.* Preparation of protein extracts, SDS/PAGE, and immunoblotting analysis were performed as described in ref. 23. Silencing of the *URA3* reporter gene was monitored by the ability of strains to grow on a medium containing 5-fluoroorotic acid as described in ref. 24.

GST Pull-Down Assays. Twenty micrograms of purified $(His)_6$-GST-fusion proteins were immobilized on reduced glutathione agarose beads and equilibrated with 200 μl of buffer H150 (20 mM Hepes-NaOH, pH 7.4/150 mM NaCl/0.5% Nonidet P-40/1 mM EDTA). One microgram of purified native chicken histones H3-H4, kindly provided by A. Prunell (Institut Jacques Monod, Paris) (25), was added to beads. Beads were washed successively with buffers identical to buffer H150 with increasing NaCl concentration up to 2 M. Bound H3 proteins were analyzed by SDS/PAGE and revealed by an antibody against the carboxyl terminus of histone H3 (Abcam, Cambridge, U.K.). $(His)_6$-GST fusion proteins were revealed by a polyclonal antibody against the $(His)_6$ tag (Novagen).

Tandem Affinity Purification (TAP) Tag Purifications of Asf1 and Asf1-V94R. pRS304-*TRP1-ASF1–13myc* and pRS304-*TRP1-asf1-V94R-13myc* were linearized with MluI and integrated at their normal chromosomal locus by transforming strain W303–1b *asf1*::*kanMX* and selecting Trp+ colonies. The 13myc tag was replaced with the TAP tag by transforming these strains with an *ASF1-TAP*::*HIS3MX6* PCR cassette. This cassette contained 111 bp of *ASF1* coding sequence upstream of the stop codon in front of the TAP sequence and 110 bp of *ASF1* 3′ noncoding sequences downstream of the *HIS3MX*6 sequence. Two liters of wild-type and *asf1-V94R* cells were grown to an optical density of 2 in a rich yeast extract/peptone/dextrose medium and the TAP-tagged proteins were purified by the standard protocol in ref. 26 after breaking cells in an Eaton press. Proteins copurifying with Asf1 were separated by SDS/PAGE and stained with Coomassie blue. The bands corresponding to Asf1 and the histones H3 and H4 were identified by a combination of mass spectrometry and immunoblotting (data not shown).

Supporting Information. A description of the DNA constructs and methods of site-specific mutagenesis used in this work is provided as *Supporting Methods*, which is published as supporting information on the PNAS web site.

Results

The Structure of the Asf1 N-Terminal Domain Is Highly Conserved. We determined the structure of the conserved N-terminal domain of human Asf1a (amino acid 1–156) by using multidimensional NMR spectroscopy (Fig. 1*a* and Table 1). The structure comprises 10 β-strands organized into an Ig-like fold composed of three β-sheets topped by two short α-helices. The ^{15}N relaxation parameters R_1, R_2, and the $^{15}N\{^1H\}$-nuclear Overhauser effect are consistent with a monomeric globular domain that presents limited internal motions with significant flexibility in the loops connecting β3-β4, β4-β5, and β8-β9 (see Fig. 6, which is published as supporting information on the PNAS web site). In contrast, the C-terminal region of human Asf1a is fully unfolded (see Fig. 7, which is published as supporting information on the PNAS web site) as indicated by the null or negative values of $^{15}N\{^1H\}$-nuclear Overhauser effects (data not shown).

The x-ray crystal structure of the N-terminal domain of *S. cerevisiae* Asf1 was recently described in ref. 16. Although the sequence of the Asf1 N-terminal domain is highly conserved (58% sequence identity between *S. cerevisiae* Asf1 and human Asf1a), some genetic data highlight functional differences. The human protein does not complement *asf1*Δ mutants of either *S. pombe* (27) *or S. cerevisiae* (data not shown), whereas the *S. cerevisiae* Asf1 N-terminal domain does complement both mutants (16, 27). The NMR solution structure of the N-terminal domain of human Asf1a superimposes well on the x-ray crystal structure of the corresponding domain from *S. cerevisiae* with a root mean square deviation of 1.78 Å for all Cα atoms and 0.83 Å for the Cα atoms of the 10 β-strands (Fig. 1*b*). The major dissimilarities are observed for the A_{48}-Y_{53} and N_{80}-G_{91} loops connecting strands β4-β5 and strands β6-β7, respectively, and the sequences of these two loops are among the most divergent regions between the human and yeast proteins (only 24% identity) (Fig. 8, which is published as supporting information on the PNAS web site). These variations may help in identifying the important factors responsible for the functional differences between the human and yeast proteins.

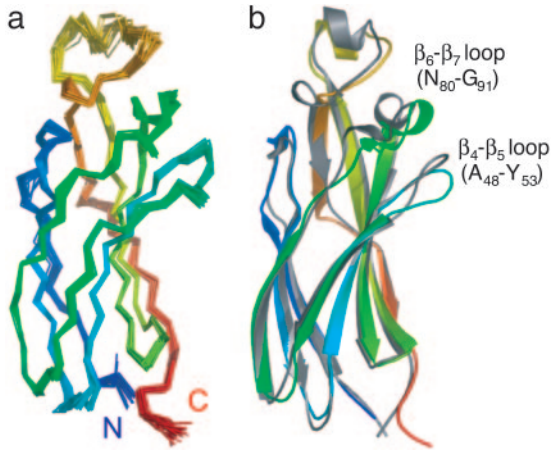

Fig. 1. The structure of the human Asf1a N-terminal domain is well conserved. (*a*) Bundle of 20 structures of human Asf1a (1–156) calculated as indicated in *Methods*. The coloring scheme indicates the relative position of the backbone atoms with the warmest colors being closest to the carboxyl terminus. (*b*) Schematic ribbon diagram (generated with PYMOL, DeLano Scientific, South San Francisco, CA) of the human Asf1a (1–156) structure closest to the mean (colored as in *a*) superimposed on the crystallographic structure of the homologous domain of *S. cerevisiae* Asf1 (16) (gray).

Interaction of Asf1 with the C-Terminal Helix of Histone H3. The histone H3/H4 complex is the best-characterized and most highly conserved partner of Asf1. However, nothing is known concerning the structural basis of this interaction or the functional pathways for which it is required. The C-terminal amino acids 97–135 of histone H3 were implicated in this interaction in a two-hybrid screen (8). This segment spans half of the helix α2 and full-length helix α3 of histone H3 in the crystal structure of the nucleosome (1). We characterized the interaction between human Asf1a and histone H3 by NMR. Addition of the H3 peptide spanning residues 97–135 to ^{15}N-Asf1a (1–156) led to line broadening due to an intermediate exchange rate, preventing further NMR characterization (data not shown). Further two-hybrid analyses indicated that shorter H3 C-terminal peptides could still interact with Asf1a (data not shown). We thus tried the shortened H3 C-terminal peptide (amino acid 122–135) in our NMR experiments and found that it led to significant variations in the Asf1 ^{15}N-HSQC spectrum with a rapid exchange rate (Fig. 2*a*). Transposing the mean square chemical shift variation upon titration (Fig. 2*b*) on the protein structure revealed a well defined binding surface on Asf1 located in a concave groove of the protein (Fig. 3). This groove is highly conserved, principally hydrophobic with residue V94 at its

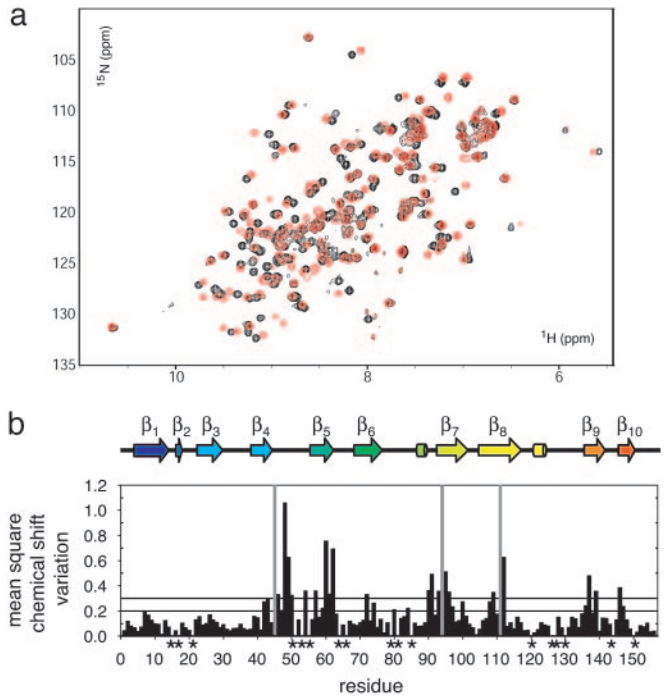

Fig. 2. Interaction of human Asf1a (1–156) with histone H3 (122–135). (*a*) Superposition of the HSQC spectrum of human Asf1a (1–156) (80 μM) with (red) and without (black) an excess of histone H3 (122–135) (160 μM) at 298 K. (*b*) Mean-square chemical shift variation calculated as described in *Methods* for human Asf1a (1–156) upon binding of H3 (122–135) as a function of the sequence. Horizontal lines at 0.2 and 0.3 show the cutoff for the color-coded representation of the protein surface in Fig. 3. The chemical exchange rate was rapid for most of the residues except the highly affected residues 45, 94, and 111, indicated with a vertical gray bar, that exhibited an intermediate exchange rate and severe line broadening due to chemical exchange that led to their absence from the ^{15}N-HSQC spectrum of the complex. Stars indicate missing values (proline residues or unassigned because of signal overlaps).

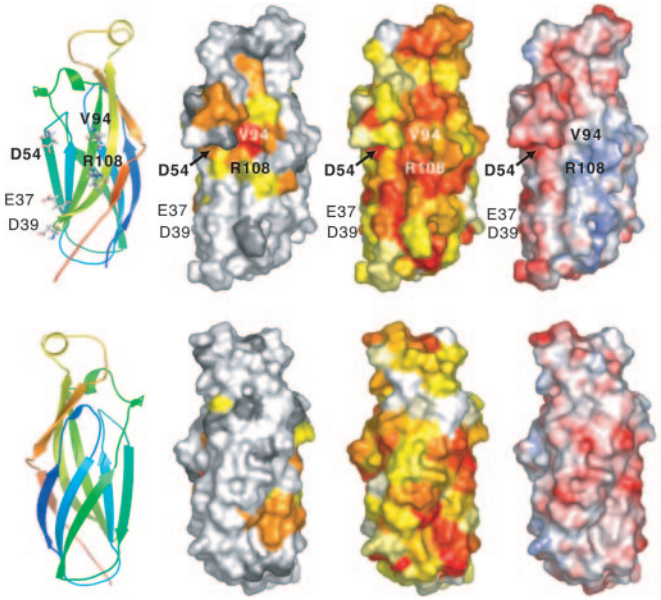

Fig. 3. Structure mapping of the chemical shift variation of Asf1a upon H3 (122–135) binding. Two orientations of the protein are presented in *Upper* and *Lower*. (*Left*) Ribbon representation of the protein. (*Left Center*) Surface color-coded representation of the mean-square chemical shift variation of Asf1a upon H3 (122–135) binding. The three line-broadened residues are shown in red, residues with $\Delta\delta > 0.3$ in orange, residues with $0.2 < \Delta\delta < 0.3$ in yellow, residues with $\Delta\delta < 0.2$ in white and undetermined residues in gray. (*Right Center*) Surface color-coded representation of the residue conservation of Asf1. The conservation was determined by using the RATE4SITE program (38) based on an alignment of 17 Asf1 sequences. The color code is a gradient from red (fully conserved residues) to white (unconserved residues). (*Right*) Color-coded representation of the electrostatic potential of human Asf1a. The potential was calculated with the software APBS (39). The color code is red for negative values, white for near zero values, and blue for positive values. Figures were generated with PYMOL, and residues mutated in this work are labeled.

center, and surrounded by polar and charged residues such as D54 and R108 (Fig. 3).

The conformation of H3 (122–135) was investigated with an ^{15}N-labeled peptide. In the absence of Asf1a, the peptide was unfolded as revealed by the reduced dispersion of the HSQC spectrum (Fig. 4*a*) and by the Hα chemical shift index (Fig. 4*b*). Large chemical shift variations were observed upon addition of unlabeled Asf1a (1–156) (Fig. 4 *a* and *c*), and the ^{15}N-H3 (122–135) peptide adopted a helical conformation from residues 122 to 131 (Fig. 4*b*) that corresponds to the C-terminal helix α3 of H3 found in the nucleosome core particle (1). The ^{15}N{^{1}H}-nuclear Overhauser effect values of the bound peptide are consistent with a structure as rigid as the Asf1a core domain (Figs. 4*d* and 6*d*) and indicate a specific binding interaction with Asf1a. Based on titration experiments, the affinity of the peptide for Asf1a (1–156) was measured to be 100 $\pm$ 20 μM.

***In Vitro* Analysis of Asf1a Binding to the Purified Histone H3/H4 Complex.** Our NMR experiments identified a site on the surface of Asf1a that was involved in binding the 13 C-terminal residues of histone H3 and was thus likely to be involved in binding the histone H3/H4 complex (Fig. 3). We made Asf1a mutants within this site in the context of GST fusion proteins to test their ability to bind the H3/H4 complex *in vitro*. The V94R mutant was chosen because it converts a conserved exposed hydrophobic residue at the center of the H3 (122–135) binding site into a positively charged arginine residue. The D54R and R108E mutants reversed the charge of two conserved residues whose chemical shift was perturbed by the H3 peptide and that are found at either side of the hydrophobic groove containing V94. Finally, a D37R+E39R double mutant was made, affecting two acidic residues that reside within a known HirA-interacting region (16) that is outside of the putative H3-binding site to compare its effect to that of the three mutants within the H3 binding site. All these residues are highly conserved and are identical in the human and the yeast proteins (Fig. 8). We also verified that the HSQC spectra of the four Asf1a (1–156) mutants were nearly superimposable with that of the wild type (data not shown), indicating that these surface mutations do not affect their global folding and structural integrity.

We used a GST pull-down assay to study the binding of wild-type and mutant Asf1a proteins (D37R+E39R, D54R, V94R, and R108E) to histone H3 within purified chicken histone H3/H4 complex (Fig. 5*a*). This native histone complex can form $(H3\text{-}H4)_2$ tetrameric particles when assembled onto DNA (25). Wild-type Asf1a and the D37R+E39R mutant strongly bound H3 within the H3/H4 complex. In contrast, the V94R mutation nearly completely abolished H3 binding, whereas the D54R mutation, and to a lesser extent the R108E mutation, partially inhibited the binding.

The inability of the Asf1a-V94R mutant to bind histones was confirmed by two independent methods. First, we added Asf1-V94R to the ^{15}N-H3 122–135 peptide and found that it was unable to induce helical formation of the H3 peptide (Fig. 9, which is published as supporting information on the PNAS web site). This finding shows that the induced helical conformation

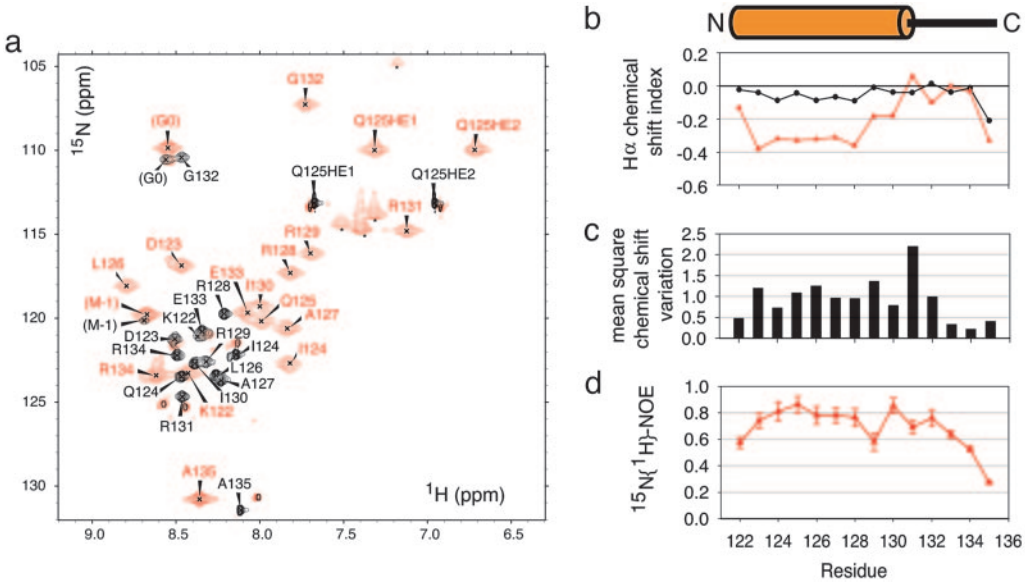

Fig. 4. H3 (122–135) folds into the native structure upon Asf1a binding. (*a*) Superposition of the ^{15}N-HSQC spectrum of ^{15}N-labeled H3 (122–135) (200 μM) with (red) and without (black) an excess of unlabeled human Asf1a (1–156) (250 μM) at 283 K. At this temperature, the chemical exchange rate was slow compared with the chemical shift variations. G_0 and M_{-1} indicate the two amino acids N-terminal to the H3 (122–135) sequence that were required for cloning the sequence in the *E. coli* expression vector as described in *Methods*. (*b*) Hα chemical shift index [$\delta_{H\alpha}^{exp}$-$\delta_{H\alpha}^{RC}$, where exp and RC refer to the experimental and random coil values, respectively, (40)] of the free (black) and bound (red) H3 (122–135). The orange cylinder shows the position of the native C-terminal α3 helix of H3 as observed in the structure of the nucleosome (1). (*c*) Mean square chemical shift variation calculated as described in *Methods* of ^{15}N-H3 (122–135) upon binding of human Asf1a (1–156) as a function of the sequence. (*d*) Heteronuclear ^{15}N{^{1}H}-nuclear Overhauser effect of the bound H3 (122–135).

of the peptide results from a highly specific interaction with the Asf1 surface identified by chemical shift mapping and centered on V94. Second, we transposed the wild type and the V94R mutant in the context of a TAP (tandem affinity purification)-tagged version of the *S. cerevisiae* Asf1 protein. Consistent with previous work (14), the histones H3 and H4 were major partners that copurified with wild-type Asf1 through tandem affinity purification. In contrast, no H3 or H4 was associated with the Asf1-V94R mutant (Fig. 5*b*). This result confirms the strong histone-binding defect of the V94R mutant.

***In Vivo* Analysis of *asf1* Mutants.** We examined the *in vivo* effects of mutations within the histone H3 or Hir binding sites of Asf1 by making V94R, D54R, R108E, D54R+R108E, and D37R+E39R mutants of the *S. cerevisiae* Asf1 protein and testing their ability to complement the phenotypes of *asf1*Δ mutants. In *S. cerevisiae*, *asf1*Δ mutants are viable, but they are temperature-sensitive for growth at 37°C (Fig. 5*d*), are highly sensitive to DNA-damaging agents that create DNA double-strand breaks (4, 13, 14), and they show defects in transcriptional silencing (9, 10, 12, 24, 28, 29). We used camptothecin and hydroxyurea as genotoxic stresses for the *asf1*Δ mutant. Camptothecin is an anticancer agent that stabilizes the covalent intermediary formed between DNA and topoisomerase I during its enzymatic relaxation of DNA (30). Collision of replication forks with these complexes leads to DNA double-strand breaks. Hydroxyurea depletes dNTP pools by inhibiting ribonucleotide reductase. Prolonged fork stalling is also thought to lead to DNA double-strand breaks (31). To examine transcriptional silencing, we used strains containing the *URA3* gene reporter inserted at three different silenced loci: the chromosome VIIL telomere (*TEL*::*URA3*) and the *HMR*a (*HMR*a::*URA3*) and *HML*α (*HML*α::*URA3*) silent mating-type cassettes. Transcriptional repression is stronger at the *HMRa* and *HML*α silent mating cassettes compared with the telomeres (32). The single *asf1*Δ mutant has only weak silencing defects, whereas *asf1*Δ *cac*Δ double mutants have strong silencing defects (9, 10, 12, 24). We thus tested transcriptional silencing in an *asf1*Δ *TEL*::*URA3* strain, as well as in *asf1*Δ *cac2*Δ double-mutant strains containing the *TEL*::*URA3*, *HMRa*::*URA3*, and *HML*α::*URA3* gene reporters. Expression of wild-type Asf1 containing a 13myc epitope fused to its carboxyl terminus from its endogenous promoter on a centromeric plasmid complemented the *asf1*Δ mutant phenotypes (Fig. 5 *d* and *e*). We then tested the function of the five Asf1 mutants in this same context. All of the mutant proteins were stably expressed in yeast at approximately the same level as the wild-type protein (Fig. 5*c*). The Asf1-V94R mutant was unable to complement any of the *asf1*Δ phenotypes. The R108E, D54R, and D54R+R108E mutants showed a graded increase in defective function. The Asf1-R108E mutant was indistinguishable from the wild-type protein in all phenotypic tests but one: it complemented the telomeric silencing defect of the *asf1*Δ *cac2*Δ double mutant slightly less than the wild-type protein (Fig. 5*e*). The Asf1-D54R mutant efficiently complemented the DNA damage sensitivity and growth defects of the *asf1*Δ mutant but appeared to function less than the wild type and Asf1-R108E mutant in all silencing strains. Finally, the D54R+R108E double mutant was clearly more defective than either single mutant in that it showed some detectable sensitivity to genotoxic stress and to growth at 37°C, as well as being totally deficient in silencing function (Fig. 5 *d* and *e*). The strong thermosensitive growth defect of the V94R mutant and the weak defect of the D45R+R108E double mutant were not due to proteolysis of the mutant proteins at 37°C (Fig. 5*c*). In conclusion, mutants defective in histone H3/H4 binding *in vitro* also showed defects in transcriptional silencing and were sensitive to DNA damaging agents and to growth at high temperatures. The severity of the phenotypes for each mutant *in vivo* was nicely correlated with the severity of their histone H3 binding defects *in vitro*.

In contrast to the H3 binding mutants, the Asf1-D37R+E39R double mutant showed silencing defects but no sensitivity to DNA damaging agents or to growth at high temperatures. These phenotypes are in agreement with those reported for a very similar Asf1-H36R+D37R double mutant. The homologous

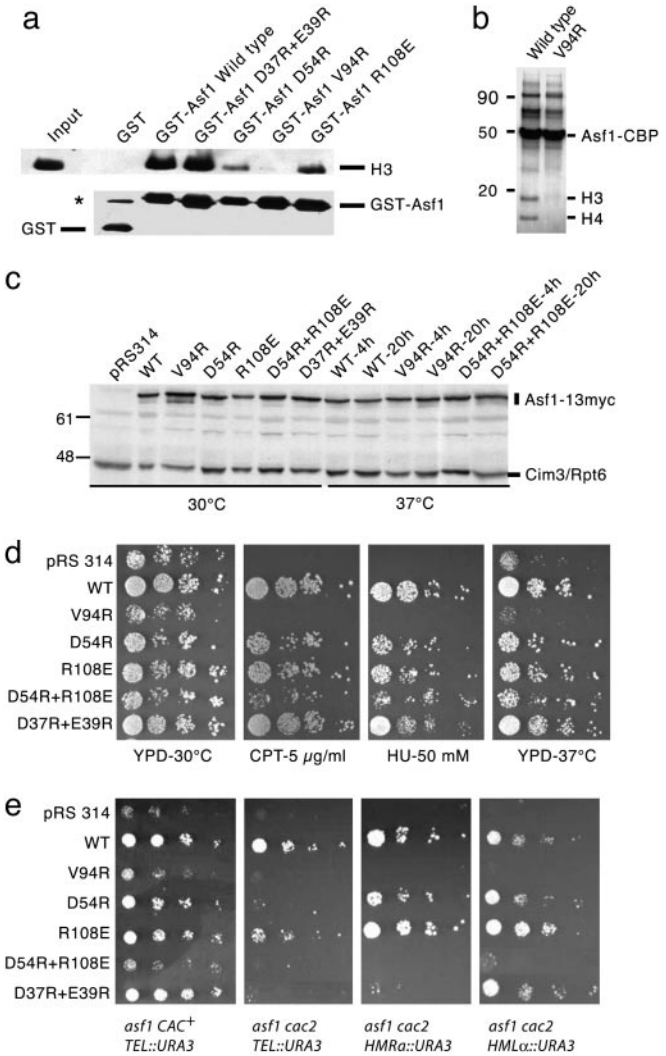

Fig. 5. *In vitro* and *in vivo* analysis of Asf1 mutants. (*a*) V94R, D54R, and R108E are involved in the binding of Asf1 to the histone H3/H4 complex. Equal amounts of purified recombinant $(His)_6$-GST, $(His)_6$-GST-Asf1a (1–156), and the indicated mutants were bound to glutathione agarose beads. *Lower* is an anti-GST immunoblot showing the equal quantities of fusion protein bound to the beads. A small quantity of the $(His)_6$-GST control protein appears as a dimerized species that migrates near the position of the $(His)_6$-GST-Asf1a proteins (indicated with a star). Binding of histone H3 within H3/H4 complexes to the GST proteins is shown in *Upper*. H3 was visualized by immunoblotting with anti-H3 antibodies. Input shows the amount of histone used for each binding reaction. (*b*) Coomassie blue-stained gel of wild-type Asf1-TAP and Asf1-V94R-TAP purified from yeast cell extracts by using the tandem affinity purification protocol. (*c*) Wild-type and mutant Asf1–13myc proteins are expressed at similar levels in yeast. The UCC6562 *asf1*Δ strain was transformed with pRS314 (*CEN-TRP1*) or pRS314 plasmids containing DNA fragments, allowing expression from the endogenous *ASF1* promoter of wild-type (WT) or mutant Asf1–13myc proteins as indicated. Protein extracts from exponentially growing cells at 30°C or from cells transferred to 37°C for 4 or 20 h as indicated were analyzed by immunoblotting with anti-myc antibodies to visualize the tagged Asf1 proteins. Asf1–13myc migrated as a closely spaced doublet of bands at ≈75 kDa. The quantity of the faster-migrating band varied between experiments, but no reproducible difference in the ratio of the two forms was seen between the wild type and any of the mutants. After developing the anti-myc blot, membranes were incubated with anti-Cim3/Rpt6 antiserum directed against a 45-kDa subunit of the 26S proteasome to verify that equal quantities of protein extract were loaded in each lane. (*d*) Sensitivity of *asf1* mutants to genotoxic stress and to growth at 37°C. UCC6562 *asf1*Δ strains transformed with the pRS314 plasmids allowing the expression of wild-type and mutant Asf1–13myc proteins described in *a* were grown to early stationary phase in synthetic complete medium without tryptophan to maintain selection for the pRS314 plasmids. The 10-fold serial dilutions of cultures were then spotted on yeast extract/peptone/dextrose plates, containing where indicated 5 μg/ml camptothecin (CPT) or 50 mM hydroxyurea (HU) and incubated at 30°C to test for sensitivity to genotoxic stress or at 37°C to test for thermosensitive growth. (*e*) The same pRS314 plasmids described above were used to test the transcriptional silencing function of the indicated wild-type and mutant Asf1–13myc proteins. These plasmids were transformed into four different silencing reporter strains: UCC6562 (*asf1 CAC+ TEL::URA3*) tests telomeric silencing in an *asf1 CAC+* background, CMY1317 (*asf1 cac2 TEL::URA3*) tests telomeric silencing in an *asf1 cac2* double-mutant background, CMY1314 (*asf1 cac2 HMRa::URA3*) tests silencing at *HMRa* in an *asf1 cac2* background, and CMY1312 (*asf1 cac2 HMLα::URA3*) tests silencing at *HMLα* in an *asf1 cac2* background. Strains were grown to early stationary phase in synthetic complete medium without tryptophan to select for the plasmid, and 10-fold dilutions of the cultures were then spotted on plates containing 5-fluoroorotic acid (5-FOA). Repression of the *URA3* reporter gene by transcriptional silencing allows growth on the FOA plates (24).

Asf1a-H36R+D37R mutant was defective in HirA binding *in vitro* (16). Interestingly, the Asf1-D37R+E39R mutant showed residual silencing function that was clearly superior to that of the Asf1-V94R and Asf1-D54R+R108E mutants in the context of the *asf1*Δ *TEL::URA3* and *asf1*Δ *cac2*Δ *HMLα*::URA3 strains. Overall, these results suggest that the Asf1-H3/H4 interaction is required for silencing at telomeres and at both silent mating cassettes.

Discussion

Characteristics of the Asf1-H3/H4 Binding Mode. We identified crucial Asf1 residues involved in the recognition of the H3/H4 complex, and we showed that the carboxyl terminus of H3 bound to Asf1 adopts a native helical conformation. Our NMR and mutational analyses suggest that the H3 C-terminal sequence is a crucial part of its interaction with the H3/H4 complex. Disrupting this interaction with the Asf1-V94R mutation prevents both interaction with the H3 C-terminal peptide and binding to the intact H3/H4 complex. Neutralization of the highly basic core histones either by using high salt concentration or adding polyacidic peptides allows assembly of core histones and DNA into nucleosome core particles *in vitro* (33, 34). It was thus reasonable to assume that electrostatic interactions would be crucial components in the interaction of physiological chaperones with core histones and, indeed, several such chaperones contain blocks of acidic sequences that may serve this role, although these acidic domains in chaperones such as Nap1, nucleoplasmin, and yeast Asf1 are not essential for their function as chaperones (16, 27, 33, 35, 36). Here, we show that the core of the Asf1a binding interface includes a conserved patch of hydrophobic residues. V94 is centrally located in this hydrophobic surface, whose chemical shifts were affected by the presence of the H3 C-terminal helix, and was also crucial for binding the intact H3/H4 complex *in vitro*. Furthermore, the yeast Asf1-V94R mutant exhibited a histone-binding defect and a strongly deleterious phenotype *in vivo*. Surrounding the hydrophobic core, charged residues such as D54 and R108 contributed to a lesser extent to the binding interface as revealed by the *in vitro* assays. A nonspecific long-range repulsive effect of the D54R mutation can be excluded because *in vitro*, the D37R+E39R double mutant affecting the same side of Asf1, binds histones H3/H4 identically to the wild type. Although the net charge of Asf1 has been maintained highly negative throughout evolution, only a few charged positions remain strictly conserved and include, in particular, the residues D54 and R108. Altogether, our results are consistent with a highly specific binding mode of Asf1 with histones H3/H4 involving hydrophobic interactions and strictly conserved charged positions.

BIOCHEMISTRY

Differential Roles for Histone H3 and Hir Protein Binding in Asf1 Function. Asf1 has been implicated in nucleosome assembly (4, 5, 8), in transcriptional silencing (9, 10, 12, 24, 28, 29, 37), and in the cellular response to DNA damage (13, 14). In yeast, it is also required for growth at high temperatures (Fig. 5) and for the transcriptional regulation of histone gene expression (9). Consistent with its multiple functions, Asf1 has been shown to physically and functionally interact with a large number of partners. The identification of these multiple interacting partners raises the question as to their role in the different pathways in which Asf1 functions. Like Asf1, many of these partners have been implicated in transcriptional activation, transcriptional silencing, and the DNA damage response. It is thus not possible to attribute specific functions to each Asf1 partner on the basis of the phenotype of individual null mutants. One approach that should allow a more precise delimitation of functions involves the identification and study of mutants that affect the interaction of Asf1 with specific partners. Recently, some mutants of Asf1a were described that decrease its binding to HirA *in vitro* (16). Analysis of one of the corresponding yeast mutants revealed that it was defective in transcriptional silencing but provided a normal level of resistance to genotoxic stress. These results thus suggested that the Asf1–Hir interaction contributes to transcriptional silencing but is not required for Asf1's role in the DNA damage response. In this study, we identified mutants of Asf1a with decreased affinity for histone H3/H4 complexes *in vitro*. Interestingly, we found an excellent correlation between the severity of the *in vitro* binding defects with that of the severity of the *in vivo* phenotypes of the corresponding yeast mutants, suggesting that binding of the histone H3/H4 complex is crucial for the role of Asf1 in the DNA damage response, in thermoresistant growth, and in transcriptional silencing, although we cannot rule out the possibility that these mutations also affect its interaction with some other important partner. Further work should provide a mechanistic description of how the histone chaperone activity of Asf1 contributes to these different functional pathways, and the identification of mutants specifically defective in binding to the remaining Asf1 partners should allow an assessment of their respective roles in these pathways.

We thank Ariel Prunell for his generous gift of purified chicken histone H3/H4 complex and for his extensive advice on histone modifications and purification, Vaughn Jackson for discussions, Dan Gottschling for the gift of silencing reporter strains, Joël Couprie, Sophie Zinn-Justin, and Bernard Gilquin for constructive discussions and precious technical support, Hervé Desvaux and Patrick Berthault for their expert NMR assistance, Carine van Heijenoort for valuable comments on the manuscript, and Geneviève Almouzni for her enthusiasm and encouragement. This work was supported by a Programme Incitatif et Coopératif of the Commissariat à l'Energie Atomique/Institut Curie on Epigenetic parameters in DNA damage response and the cell cycle, funds for the Structural Radiobiology efforts of the Common NMR Laboratory of the Commissariat à l'Energie Atomique/Saclay, and Association pour la Recherche sur le Cancer Grant 4470 (to C.M.). A.L. and B.A. are supported by a Direction Générale des Armées fellowship.

1. Luger, K., Mader, A. W., Richmond, R. K., Sargent, D. F. & Richmond, T. J. (1997) *Nature* **389,** 251–260.
2. Loyola, A. & Almouzni, G. (2004) *Biochim. Biophys. Acta* **1677,** 3–11.
3. Verreault, A. (2000) *Genes Dev.* **14,** 1430–1438.
4. Tyler, J. K., Adams, C. R., Chen, S. R., Kobayashi, R., Kamakaka, R. T. & Kadonaga, J. T. (1999) *Nature* **402,** 555–560.
5. Mello, J. A., Sillje, H. H., Roche, D. M., Kirschner, D. B., Nigg, E. A. & Almouzni, G. (2002) *EMBO Rep.* **3,** 329–334.
6. Tagami, H., Ray-Gallet, D., Almouzni, G. & Nakatani, Y. (2004) *Cell* **116,** 51–61.
7. Adkins, M. W. & Tyler, J. K. (2004) *J. Biol. Chem.* **279,** 52069–52074.
8. Munakata, T., Adachi, N., Yokoyama, N., Kuzuhara, T. & Horikoshi, M. (2000) *Genes Cells* **5,** 221–233.
9. Sutton, A., Bucaria, J., Osley, M. A. & Sternglanz, R. (2001) *Genetics* **158,** 587–596.
10. Sharp, J. A., Fouts, E. T., Krawitz, D. C. & Kaufman, P. D. (2001) *Curr. Biol.* **11,** 463–473.
11. Tyler, J. K., Collins, K. A., Prasad-Sinha, J., Amiott, E., Bulger, M., Harte, P. J., Kobayashi, R. & Kadonaga, J. T. (2001) *Mol. Cell. Biol.* **21,** 6574–6584.
12. Krawitz, D. C., Kama, T. & Kaufman, P. D. (2002) *Mol. Cell. Biol.* **22,** 614–625.
13. Hu, F., Alcasabas, A. A. & Elledge, S. J. (2001) *Genes Dev.* **15,** 1061–1066.
14. Emili, A., Schieltz, D. M., Yates, J. R., 3rd, & Hartwell, L. H. (2001) *Mol. Cell* **7,** 13–20.
15. Sillje, H. H. & Nigg, E. A. (2001) *Curr. Biol.* **11,** 1068–1073.
16. Daganzo, S. M., Erzberger, J. P., Lam, W. M., Skordalakes, E., Zhang, R., Franco, A. A., Brill, S. J., Adams, P. D., Berger, J. M. & Kaufman, P. D. (2003) *Curr. Biol.* **13,** 2148–2158.
17. Mousson, F., Couprie, J., Thuret, J. Y., Neumann, J. M., Mann, C. & Ochsenbein, F. (2004) *J. Biomol. NMR* **29,** 413–414.
18. Linge, J. P., Habeck, M., Rieping, W. & Nilges, M. (2003) *Bioinformatics* **19,** 315–316.
19. Nilges, M., Macias, M. J., O'Donoghue, S. I. & Oschkinat, H. (1997) *J. Mol. Biol.* **269,** 408–422.
20. Cornilescu, G., Delaglio, F. & Bax, A. (1999) *J. Biomol. NMR* **13,** 289–302.
21. Vuister, G. W. & Bax, A. (1994) *J. Biomol. NMR* **4,** 193–200.
22. Farmer, B. T., 2nd, Constantine, K. L., Goldfarb, V., Friedrichs, M. S., Wittekind, M., Yanchunas, J., Jr., Robertson, J. G. & Mueller, L. (1996) *Nat. Struct. Biol* **3,** 995–997.
23. Dubacq, C., Chevalier, A. & Mann, C. (2004) *Mol. Cell. Biol.* **24,** 2560–2572.
24. Singer, M. S., Kahana, A., Wolf, A. J., Meisinger, L. L., Peterson, S. E., Goggin, C., Mahowald, M. & Gottschling, D. E. (1998) *Genetics* **150,** 613–632.
25. Hamiche, A., Carot, V., Alilat, M., De Lucia, F., O'Donohue, M. F., Revet, B. & Prunell, A. (1996) *Proc. Natl. Acad. Sci. USA* **93,** 7588–7593.
26. Puig, O., Caspary, F., Rigaut, G., Rutz, B., Bouveret, E., Bragado-Nilsson, E., Wilm, M. & Seraphin, B. (2001) *Methods* **24,** 218–229.
27. Umehara, T., Chimura, T., Ichikawa, N. & Horikoshi, M. (2002) *Genes Cells* **7,** 59–73.
28. Meijsing, S. H. & Ehrenhofer-Murray, A. E. (2001) *Genes Dev.* **15,** 3169–3182.
29. Osada, S., Sutton, A., Muster, N., Brown, C. E., Yates, J. R., 3rd, Sternglanz, R. & Workman, J. L. (2001) *Genes Dev.* **15,** 3155–3168.
30. Connelly, J. C. & Leach, D. R. (2004) *Mol. Cell* **13,** 307–316.
31. Osborn, A. J., Elledge, S. J. & Zou, L. (2002) *Trends Cell Biol.* **12,** 509–516.
32. Rusche, L. N., Kirchmaier, A. L. & Rine, J. (2003) *Annu. Rev. Biochem.* **72,** 481–516.
33. Akey, C. W. & Luger, K. (2003) *Curr. Opin. Struct. Biol.* **13,** 6–14.
34. Stein, A., Whitlock, J. P., Jr., & Bina, M. (1979) *Proc. Natl. Acad. Sci. USA* **76,** 5000–5004.
35. Arnan, C., Saperas, N., Prieto, C., Chiva, M. & Ausio, J. (2003) *J. Biol. Chem.* **278,** 31319–31324.
36. McBryant, S. J., Park, Y. J., Abernathy, S. M., Laybourn, P. J., Nyborg, J. K. & Luger, K. (2003) *J. Biol. Chem.* **278,** 44574–44583.
37. Moshkin, Y. M., Armstrong, J. A., Maeda, R. K., Tamkun, J. W., Verrijzer, P., Kennison, J. A. & Karch, F. (2002) *Genes Dev.* **16,** 2621–2626.
38. Pupko, T., Bell, R. E., Mayrose, I., Glaser, F. & Ben-Tal, N. (2002) *Bioinformatics* **18,** S71–S77.
39. Baker, N. A., Sept, D., Joseph, S., Holst, M. J. & McCammon, J. A. (2001) *Proc. Natl. Acad. Sci. USA* **98,** 10037–10041.
40. Wishart, D. S., Sykes, B. D. & Richards, F. M. (1992) *Biochemistry* **31,** 1647–1651.